PHYSICAL REVIEW B **96**, 241106(R) (2017)

Observation of open-orbit Fermi surface topology in the extremely large magnetoresistance semimetal $MoAs_2$

R. Lou,[1] Y. F. Xu,[2,3] L.-X. Zhao,[2,3] Z.-Q. Han,[1] P.-J. Guo,[1] M. Li,[1,4] J.-C. Wang,[1] B.-B. Fu,[2,3] Z.-H. Liu,[5] Y.-B. Huang,[4] P. Richard,[2,3,6] T. Qian,[2,6] K. Liu,[1] G.-F. Chen,[2,3,6] H. M. Weng,[2,6] H. Ding,[2,3,6] and S.-C. Wang[1,*]

[1]*Department of Physics and Beijing Key Laboratory of Opto-electronic Functional Materials & Micro-nano Devices, Renmin University of China, Beijing 100872, China*

[2]*Beijing National Laboratory for Condensed Matter Physics and Institute of Physics, Chinese Academy of Sciences, Beijing 100190, China*

[3]*School of Physical Sciences, University of Chinese Academy of Sciences, Beijing 100190, China*

[4]*Shanghai Synchrotron Radiation Facility, Shanghai Institute of Applied Physics, Chinese Academy of Sciences, Shanghai 201204, China*

[5]*State Key Laboratory of Functional Materials for Informatics, SIMIT, Chinese Academy of Sciences, Shanghai 200050, China*

[6]*Collaborative Innovation Center of Quantum Matter, Beijing, China*

(Received 19 July 2017; revised manuscript received 30 September 2017; published 19 December 2017)

While recent advances in band theory and sample growth have expanded the series of extremely large magnetoresistance (XMR) semimetals in transition-metal dipnictides $TmPn_2$ (Tm = Ta, Nb; Pn = P, As, Sb), the experimental study on their electronic structure and the origin of XMR is still absent. Here, using angle-resolved photoemission spectroscopy combined with first-principles calculations and magnetotransport measurements, we performed a comprehensive investigation on $MoAs_2$, which is isostructural to the $TmPn_2$ family and also exhibits quadratic XMR. We resolve a clear band structure well agreeing with the predictions. Intriguingly, the unambiguously observed Fermi surfaces (FSs) are dominated by an open-orbit topology extending along both the [100] and [001] directions in the three-dimensional Brillouin zone. We further reveal the trivial topological nature of $MoAs_2$ by bulk parity analysis. Based on these results, we examine the proposed XMR mechanisms in other semimetals, and conclusively ascribe the origin of quadratic XMR in $MoAs_2$ to the carriers motion on the FSs with dominant open-orbit topology, innovating in the understanding of quadratic XMR in semimetals.

DOI: 10.1103/PhysRevB.96.241106

The emergence of novel states in condensed matter is not only classified by the typical spontaneous symmetry breaking, but also by their topology, i.e., the topologically protected quantum states [1–3]. The discovery of such symmetry-protected states of matter in two-dimensional (2D) [4–6] and three-dimensional (3D) topological insulators [7], node-line semimetals [8,9], topological crystalline insulators [10,11], and Dirac and Weyl semimetals [12–17], has attracted tremendous interests in condensed-matter physics and material science. The magnetotransport behavior of these states is often unusual, such as linear transverse magnetoresistance (MR) and negative longitudinal MR in Dirac and Weyl semimetals [18–24], and more generally, extremely large transverse MR (XMR) in nonmagnetic semimetals [25–30].

Recently, the discovery of XMR in a class of transition-metal dipnictides $TmPn_2$ (Tm = Ta, Nb; Pn = P, As, Sb) [31–36] has sparked immense interests for understanding the underlying mechanism of quadratic XMR and exploring novel quantum states arising from nontrivial topology. Another two series of semimetals possessing quadratic XMR behavior and rich topological characteristics are the ZrSiS family [37–39] and LnX (Ln = La, Y, Nd, or Ce; X = Sb/Bi) series [40–46], whose electronic structures have been considerably studied both in theory and experiment [47–53]. While the band structures of the $TmPn_2$ series have been theoretically characterized in several works [32–34,54], experimental observations have not yet been reported. It is widely believed that the large positive MR in semimetals is intimately related to their underlying electronic structures. Therefore, a systematic and unambiguous experimental study on the electronic structure of the $TmPn_2$ family is urgently demanded. Eventually, we suggest the open-orbit Fermi surface (FS) topology as another candidate mechanism to explain the XMR, in addition to the earlier proposed origins like nontrivial band topology [40], forbidden backscattering at zero field [55], and electron-hole compensation [56].

In this Rapid Communication, we employ systematic angle-resolved photoemission spectroscopy (ARPES), first-principles calculations, and magnetotransport measurements on $MoAs_2$, which is isostructural to the $TmPn_2$ family and exhibits quadratic MR exceeding 3.2×10^4% at 1.8 K under a 9-T magnetic field. The FS topology is clearly resolved to display two "double-ripple"-shaped FSs extending along the [100] direction (a axis), which do not close along the [001] direction (normal to the ab plane) either, and one pocket at $\bar{X}$. In addition, we identify two "handle"-like FSs around $\bar{\Gamma}$, which arise from a trivial massless surface state (SS) along $\bar{\Gamma}$-$\bar{X}$. Our detailed electronic structure of $MoAs_2$ would facilitate a more comprehensive understanding of the quadratic XMR in the $TmPn_2$ family.

High-quality single crystals of $MoAs_2$ with large residual resistance ratio [RRR = R(300 K)/R(1.8 K) = 1238] were grown via the chemical vapor transport method. Detailed methods for ARPES and first-principles calculations can be found in Sec. I of Supplemental Material (SM) [57]. $MoAs_2$ crystallizes in a monoclinic structure with space group $C2/m$ (No. 12), as illustrated in Fig. 1(a) [58]. It is isostructural to the well-known $TmPn_2$ family. Figure 1(b) shows the x-ray diffraction (XRD) pattern recorded on single crystals measured

*scw@ruc.edu.cn

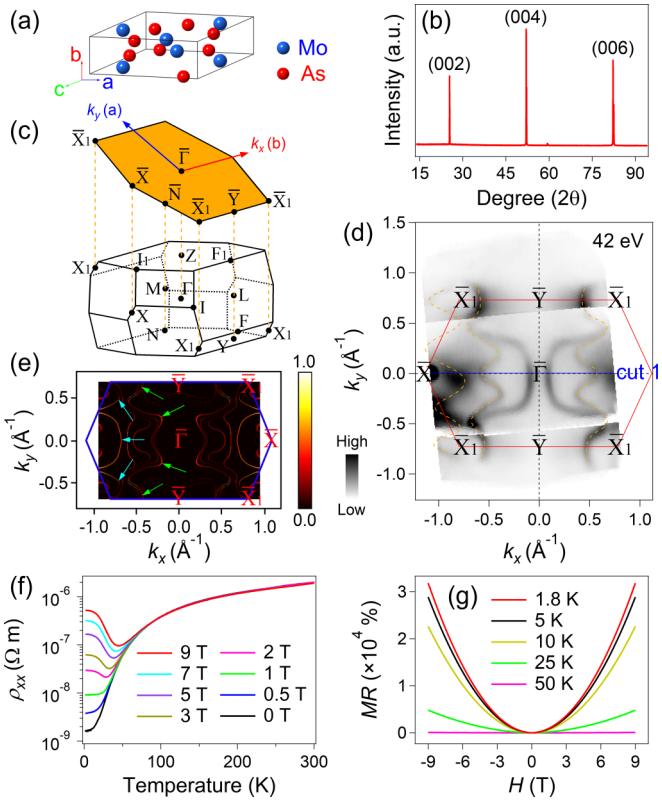

FIG. 1. (a) Schematic crystal structure of $MoAs_2$. (b) XRD pattern on the (001) surface. (c) Schematic primitive BZ and 2D projected BZ of the (001) surface. (d) Constant energy ARPES image obtained by $h\nu = 42$ eV at E_F with the mapping center around the $\bar{\Gamma}$ point. Cut 1 indicates the momentum location of the measured bands in Figs. 2(a) and 2(b). Red lines represent the (001) surface BZ. Orange dashed curves are guides to the eye for the "double-ripple"-shaped FSs. (e) Calculated FSs for a 10-unit-cell-thick (001) slab with the MoAs-terminated layer. The inner and outer "ripple"-shaped FSs are indicated by green and cyan arrows, respectively. Blue lines represent the (001) surface BZ. The intensity of the color scales the spectral weight projected to the topmost unit cell. (f) Temperature dependence of the resistivity in different magnetic fields. The magnetic field is parallel to the [001] direction and the electric current is parallel to the [010] direction (b axis). (g) $\mathrm{MR}\,(\%) = [R(H) - R(0)]/R(0) \times 100\%$ plotted as a function of magnetic field at temperatures from 1.8 to 50 K.

by ARPES, indicating our measurements were performed on the (001) plane. The schematic 3D Brillouin zone (BZ) of the primitive cell and the corresponding 2D projected BZ of the (001) surface are presented in Fig. 1(c). In Fig. 1(d), one can see the FSs measured with $h\nu = 42$ eV exhibiting obvious modulations along k_y. We observe two double-ripple-shaped FSs elongated along the [100] direction near the BZ boundary $\bar{X}$ and $\bar{X}_1$, one pocket at $\bar{X}$, as well as two handlelike FSs around $\bar{\Gamma}$. By further comparing with the calculated bulk band dispersions illustrated in Fig. 2, one can identify that the handlelike FSs are not of bulk origin, but rather derive from a nontopologically protected SS as discussed in the following. The experimental FSs are in good agreement with the slab model calculations in Fig. 1(e) [59].

Figure 1(f) is the temperature evolution of the resistivity in different magnetic fields. $MoAs_2$ shows the metallic behavior from 1.8 to 300 K without magnetic field. When the 9-T magnetic field is applied, one can see a prominent upturn and a saturation at low temperatures. As depicted in Fig. 1(g), $MoAs_2$ exhibits rather large MR exceeding $3.2 \times 10^4\%$ at 1.8 K under 9-T magnetic field, and there is a drastic suppression of MR with increasing temperature. One can obtain a nearly quadratic exponent $m = 1.97$ by fitting the MR-H profile at 1.8 K with a power-law function. These fingerprints are consistent with the common features of XMR semimetals [56].

In order to uncover the underlying nature of quadratic XMR and topological characteristics in $MoAs_2$, we investigate the near-E_F band dispersions along $\bar{\Gamma}$-$\bar{X}$ and $\bar{Y}$-$\bar{X}_1$. The band structure along $\bar{\Gamma}$-$\bar{X}$ is presented in Figs. 2(a)–2(c). As shown in Figs. 2(a) and 2(b), we identify one Dirac-cone-like band centered at $\bar{\Gamma}$ that will be discussed below. Three additional bands crossing E_F are clearly distinguished. The innermost electron band (α_1) disperses slowly and crosses E_F at $k_x \sim -0.58$ Å^{-1}, forming the inner "ripple"-shaped FS, then it turns back as the outmost electron band (α_2), which is in agreement with the bulk band calculations along Γ-X depicted in Fig. 2(c). As the absence of the middle one (α_3), which forms the outer "ripple"-shaped FS, in the calculations along Γ-X, we suggest that α_3 may not come from the $k_z = 0$ plane. Due to the short escape length of the photoelectrons excited by the vacuum ultraviolet light in our ARPES experiments, the k_z broadening effect would be prominent [60], demonstrated by previous ARPES studies [51,52,61–64]; we further perform bulk band calculations along Z-I_1 (in the $k_z = \pi$ plane) as shown in Fig. 2(c). The consistency between α_3 and the calculations helps in finding out the origin of this band [65].

We investigate the electronic structure along $\bar{Y}$-$\bar{X}_1$ to examine the origin of the double-ripple-shaped FSs. As indicated in Fig. 2(d), the double-ripple-shaped feature can be resolved more clearly from the FS mapping focusing around the $\bar{Y}$ point, while the handlelike FSs are relatively weak in this geometry due to the matrix element effect. From the measured band dispersions along $\bar{Y}$-$\bar{X}_1$ illustrated in Figs. 2(e) and 2(f), one can observe two almost linearly dispersive bands crossing E_F indicated by white arrows. These two bands are denoted as β_1 and β_2, which correspond to the inner and outer ripple-shaped FSs, respectively. Detailed energy distribution curve (EDC) analyses on β_1 and β_2 are shown in Figs. 2(j) and S3 (Sec. IV of the SM [57]), respectively. The experimental band structures agree with the slab calculations along $\bar{X}_1$-$\bar{Y}$-$\bar{X}_1$ shown in Fig. 2(g). By comparing with the bulk calculations along Y-X_1 (near the $k_z = \pi$ plane), displayed as Fig. S2(b) in Sec. III of the SM [57], the fact that α_3, which is captured by the calculations along Z-I_1 rather than Γ-X, derives from the projection of the $k_z \approx \pi$ plane due to the k_z broadening effect [51,52] can be further supported. The consistency between measured electronic structures along $\bar{Y}$-$\bar{X}_1$ and theoretical calculations can be proved by the presence of a band gap between β_1 and β_2 (see a quantitative analysis on this gap in Sec. V of the SM [57]). To further demonstrate the open character of the in-plane FSs, we study the band structure along cut 3, i.e., $k_y \sim 0.50$ Å^{-1}, the momentum where the

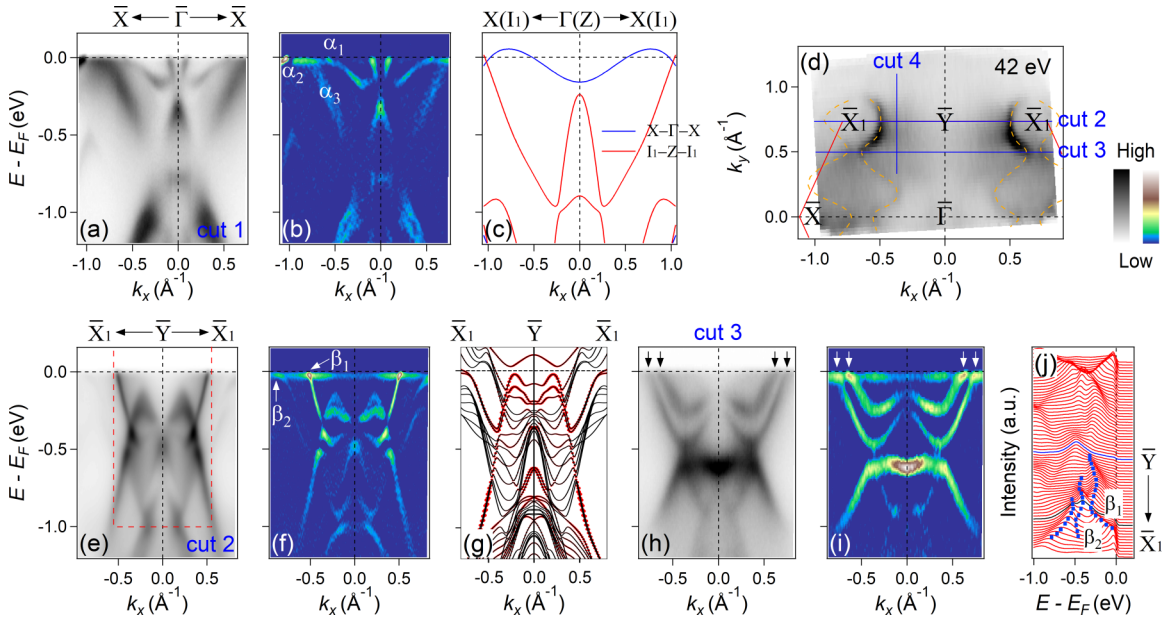

FIG. 2. (a),(b) Photoemission intensity plot and corresponding second derivative plot along $\bar{\Gamma}$-$\bar{X}$ [cut 1 in Fig. 1(d)], respectively. (c) Calculated band structures along Γ-X and Z-I_1, considering that X and I_1 points are approximately projected to one point on the (001) surface. (d) FS intensity plot obtained by integrating the spectral weight within $E_F \pm 10$ meV recorded with $h\nu = 42$ eV; the mapping center is near $\bar{Y}$ point. Cuts 2 and 3 indicate the momentum locations of the experimental band structures in (e)–(j). The electronic structures measured along cut 4 are presented in Fig. S4 (Sec. V of the SM [57]). (e),(f) Same as (a),(b) but along $\bar{Y}$-$\bar{X}_1$ [cut 2 in (d)]. Red dashed rectangle illuminates the area for EDC analysis in (j). (g) Calculated band structure along $\bar{X}_1$-$\bar{Y}$-$\bar{X}_1$ for a 10-unit-cell-thick (001) slab. (h),(i) Same as (a),(b) but along cut 3 in (d). (j) EDC plot of (e). The band gap is highlighted by a black curve. Blue dots are extracted peak positions, serving as guides to the eye.

inner and outer ripple-shaped FSs are closest to each other. In Figs. 2(h) and 2(i), as marked by vertical arrows, the two linearly dispersing bands are clearly separated at E_F.

While most experimental band structures along $\bar{\Gamma}$-$\bar{X}$ are in agreement with the bulk band calculations, we observe an extra Dirac-cone-like band centered at $\bar{\Gamma}$. To illuminate the origin of this band, we investigate the band dispersions recorded with different photon energies [66,67]. We show the constant energy plot in the k_x-k_z plane at $k_y = 0$ at E_F and $E = -0.24$ eV, which is the binding energy of the Dirac point (DP) at $\bar{\Gamma}$, in Figs. 3(a) and 3(c), respectively. The corresponding momentum distribution curve (MDC) plots are presented in Figs. 3(b) and 3(d), respectively. The Dirac-like band features, including the Fermi crossings and the DP, do not show noticeable change with a varying photon energy over a wide range, confirming that it is a SS [68].

We further perform k_z-dependent measurements along $\bar{Y}$-$\bar{X}_1$ focusing on the double-ripple-shaped FSs. The photon energy variation covers more than one BZ along the k_z direction (~ 0.88 Å^{-1}), which is sufficient to illustrate the periodicity along k_z. As shown in Figs. 4(a)–4(c), the double-ripple-shaped open FSs do not close along the k_z direction either (see Fig. S5 in Sec. VI of the SM for more manifestations of the open character [57]). When the FS topology contains open orbits along certain directions, MR in materials is not saturated and parabolically dependent on the magnetic field [69,70]. To elucidate the possible electronic origin of quadratic XMR in $MoAs_2$, angular-dependent MR measurements were carried out (see details of the experimental setup and discussions on the anisotropy of MR in Sec. VIII of the SM [57]).

So far, immense work has been generated on the origin of quadratic XMR behavior, and several mechanisms have been proposed, including nontrivial band topology [40], forbidden backscattering at zero field [55], and electron-hole compensation [56]. First, the field-induced resistivity upturn and plateau is suggested as the consequences of breaking time-reversal symmetry in topological semimetals [40], whereas the Z_2 classification of $MoAs_2$ is (0; 000) [71] based on our first-principles calculations (detailed analysis can be found in Sec. VII of the SM [57]), demonstrating that $MoAs_2$ is a topologically trivial material. This excludes the possibility that the XMR in $MoAs_2$ is associated with nontrivial band topology. Second, the spin degeneracy is removed by spin-orbit coupling due to the lack of inversion symmetry in WTe_2, leading to an exotic spin texture of the bands, which has been claimed to play an important role in the XMR of WTe_2 [55]. This explanation is not applicable to $MoAs_2$ either, because the inversion symmetry in $MoAs_2$ preserves that its spins are doubly degenerate at zero field. Third, while electron-hole compensation can be broadly applied in many XMR semimetals with closed FS trajectories based on the two-band model [41,51,56,72], its availability in XMR materials with open FSs is still unclear [73]. From another perspective, it should be noted that the MR tends to a constant, i.e., it saturates, in high fields for FSs consisting of closed electron and hole pockets, unless they have exactly equal volume. This contrasts with the MR for open FSs, which increases as H^2

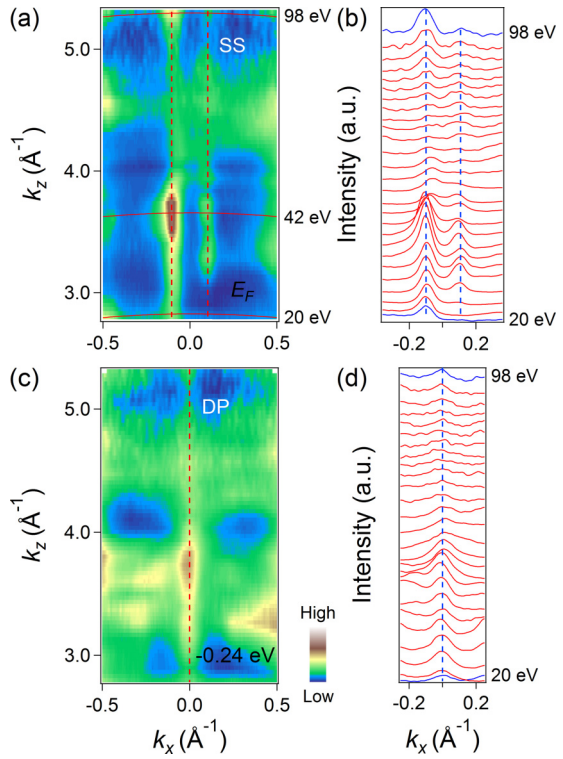

FIG. 3. (a) ARPES intensity map at E_F in the k_x-k_z plane at $k_y = 0$ recorded with various photon energies. (b) MDCs of (a) around the BZ center. (c) Same as (a) but at $E = -0.24$ eV. (d) MDCs of (c) around the BZ center. Red and blue dashed lines in (a),(b) and (c),(d) show the Fermi crossings and the DP of the SS around $\bar{\Gamma}$, where identifiable, respectively.

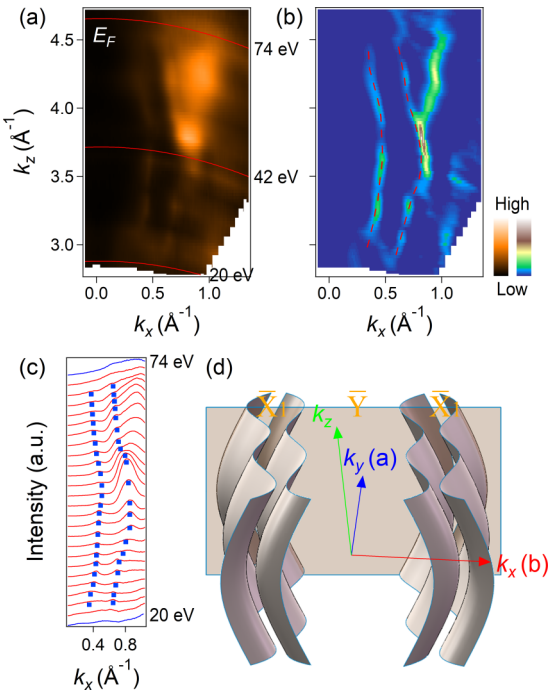

FIG. 4. (a) ARPES intensity map at E_F in the k_x-k_z plane at $k_y = \pi$ recorded with various photon energies. (b) Second derivative plot of (a). (c) MDCs of (a). Red dashed curves in (b) and blue dots in (c), which are extracted peak positions, indicate the Fermi crossings of the k_z band map. (d) Schematic diagram of the open FSs extending in the 3D BZ. The translucent plane indicates the momentum location of the k_x-k_z mapping in (a).

and exhibits nonsaturation without the restriction of carrier compensation [74]. For the former, under the influence of a magnetic field, carriers in clean materials with closed FSs will travel several orbits before getting scattered, resulting in velocity average to zero in the plane perpendicular to the magnetic field. As for the carriers on open FSs, the product of the cyclotron frequency (ω_c) and the relaxation time (τ) is no longer much larger than 1, thus leading to a finite in-plane velocity. These two conditions cause the above two distinct field dependences [69,70]. Since the dominant open-orbit FS topology can, by itself, lead to the quadratic XMR in $MoAs_2$, while the dominant closed FSs are necessary for the nonsaturated MR induced by carrier compensation, thus, the electron-hole compensation mechanism cannot be applied to the XMR in $MoAs_2$.

Hence, it is reasonable to suggest that the quadratic XMR in $MoAs_2$ is attributed to the carriers motion on the FSs with dominant open-orbit topology. Furthermore, despite what topology the FSs are, the ultrahigh charge mobilities are the key condition effectively enhancing the MR in semimetals [41,70]; this is also applicable in $MoAs_2$, of which μ_e and μ_h is 1.04 and 3.49 $\times 10^4 \mathrm{cm}^2\,\mathrm{V}^{-1}\,\mathrm{s}^{-1}$, respectively. They are determined by fitting the Hall conductivity at $T = 1.8$ K using the two-carrier model [75,76], as illustrated in Fig. S1(b) (Sec. II of the SM [57]). The open FS character along certain directions has also been observed in $PdCoO_2$ and ZrSiS exhibiting the XMR behavior [77–79]. However, for $PdCoO_2$, the field dependence of MR is not parabolic and the role of open FSs on the XMR has not yet been studied [77]; for ZrSiS, the carrier compensation is proposed to be dominant in the quadratic XMR when $H \parallel [001]$, while the open-orbit FS topology serves to enhance the MR ($\sim$50%) when $H \parallel [011]$, as for the existence of open FSs when $H \parallel [010]$ [79].

In conclusion, we present the comprehensive electronic structure of XMR semimetal $MoAs_2$. The observed FSs are dominated by open-orbit topology extending along both the [100] and [001] directions. We demonstrate the trivial topological nature of $MoAs_2$ by bulk parity analysis. Our results unambiguously suggest that the origin of quadratic XMR in $MoAs_2$ is attributed to the carriers motion on the FSs with dominant open-orbit topology, serving as a novel mechanism for XMR in semimetals.

We would like to thank H. C. Lei and T.-L. Xia for fruitful discussions, and Y.-Y. Wang and S.-S. Sun for their help in transport measurements. This work was supported by the Ministry of Science and Technology of China (Programs No. 2013CB921700, No. 2015CB921000, No. 2016YFA0300300, No. 2016YFA0300600, No. 2016YFA0302400, and No. 2016YFA0401000), the National Natural Science Foundation of China (Grants No. 11774421, No. 11274381, No. 11274362, No. 11474340, No. 11234014, No. 11274367, No. 11474330, No. 11674371, and No. 11704394), and the Chinese Academy of Sciences (CAS) (Project No. XDB07000000). R.L., K.L.,

and J.W. were supported by the Fundamental Research Funds for the Central Universities, and the Research Funds of Renmin University of China (RUC) (Grants No. 17XNH055, No. 14XNLQ03, and No. 17XNLF06). Z.L. was supported by the Shanghai Sailing Program (Grant No. 17YF1422900). Y.H. was supported by the CAS Pioneer Hundred Talents Program.

R.L., Y.F.X., L.-X.Z., and Z.-Q.H. contributed equally to this work.

[1] M. Z. Hasan and C. L. Kane, Rev. Mod. Phys. **82**, 3045 (2010).
[2] X.-L. Qi and S.-C. Zhang, Rev. Mod. Phys. **83**, 1057 (2011).
[3] H. Weng, X. Dai, and Z. Fang, MRS Bull. **39**, 849 (2014).
[4] B. A. Bernevig, T. L. Hughes, and S.-C. Zhang, Science **314**, 1757 (2006).
[5] M. König, S. Wiedmann, C. Brüne, A. Roth, H. Buhmann, L. W. Molenkamp, X.-L. Qi, and S.-C. Zhang, Science **318**, 766 (2007).
[6] I. Knez, R.-R. Du, and G. Sullivan, Phys. Rev. Lett. **107**, 136603 (2011).
[7] Y. L. Chen, J. G. Analytis, J.-H. Chu, Z. K. Liu, S.-K. Mo, X. L. Qi, H. J. Zhang, D. H. Lu, X. Dai, Z. Fang, S. C. Zhang, I. R. Fisher, Z. Hussain, and Z.-X. Shen, Science **325**, 178 (2009).
[8] A. A. Burkov, M. D. Hook, and L. Balents, Phys. Rev. B **84**, 235126 (2011).
[9] R. Yu, H. M. Weng, Z. Fang, X. Dai, and X. Hu, Phys. Rev. Lett. **115**, 036807 (2015).
[10] L. Fu, Phys. Rev. Lett. **106**, 106802 (2011).
[11] T. H. Hsieh, H. Lin, J. Liu, W. Duan, A. Bansil, and L. Fu, Nat. Commun. **3**, 982 (2012).
[12] Z. Wang, Y. Sun, X.-Q. Chen, C. Franchini, G. Xu, H. Weng, X. Dai, and Z. Fang, Phys. Rev. B **85**, 195320 (2012).
[13] Z. K. Liu, B. Zhou, Y. Zhang, Z. J. Wang, H. Weng, D. Prabhakaran, S.-K. Mo, Z. X. Shen, Z. Fang, X. Dai, Z. Hussain, and Y. L. Chen, Science **343**, 864 (2014).
[14] H. Weng, C. Fang, Z. Fang, B. A. Bernevig, and X. Dai, Phys. Rev. X **5**, 011029 (2015).
[15] B. Q. Lv, H. M. Weng, B. B. Fu, X. P. Wang, H. Miao, J. Ma, P. Richard, X. C. Huang, L. X. Zhao, G. F. Chen, Z. Fang, X. Dai, T. Qian, and H. Ding, Phys. Rev. X **5**, 031013 (2015).
[16] S. Huang, S. Xu, I. Belopolski, C. Lee, G. Chang, B. Wang, N. Alidoust, G. Bian, M. Neupane, C. Zhang, S. Jia, A. Bansil, H. Lin, and M. Z. Hasan, Nat. Commun. **6**, 7373 (2015).
[17] S. Xu, I. Belopolski, N. Alidoust, M. Neupane, G. Bian, C. Zhang, R. Sankar, G. Chang, Z. Yuan, C. Lee, S. Huang, H. Zheng, J. Ma, D. Sanchez, B. Wang, A. Bansil, F. Chou, P. Shibayev, H. Lin, S. Jia, and M. Z. Hasan, Science **349**, 613 (2015).
[18] J. Feng, Y. Pang, D. Wu, Z. Wang, H. Weng, J. Li, X. Dai, Z. Fang, Y. Shi, and L. Lu, Phys. Rev. B **92**, 081306(R) (2015).
[19] T. Liang, Q. Gibson, M. N. Ali, M. Liu, R. J. Cava, and N. P. Ong, Nat. Mater. **14**, 280 (2015).
[20] X. C. Huang, L. X. Zhao, Y. J. Long, P. P. Wang, D. Chen, Z. H. Yang, H. Liang, M. Q. Xue, H. M. Weng, Z. Fang, X. Dai, and G. F. Chen, Phys. Rev. X **5**, 031023 (2015).
[21] C. Shekhar, A. K. Nayak, Y. Sun, M. Schmidt, M. Nicklas, I. Leermakers, U. Zeitler, Z. K. Liu, Y. L. Chen, W. Schnelle, J. Grin, C. Felser, and B. H. Yan, Nat. Phys. **11**, 645 (2015).
[22] J. Xiong, S. K. Kushwaha, T. Liang, J. W. Krizan, M. Hirschberger, W. Wang, R. J. Cava, and N. P. Ong, Science **350**, 413 (2015).
[23] C. Zhang, S.-Y. Xu, I. Belopolski, Z. Yuan, Z. Lin, B. Tong, N. Alidoust, C.-C. Lee, S.-M. Huang, H. Lin, M. Neupane, D. S. Sanchez, H. Zheng, G. Bian, J. Wang, C. Zhang, T. Neupert, M. Z. Hasan, and S. Jia, Nat. Commun. **7**, 10735 (2016).
[24] C.-Z. Li, L. Wang, H. W. Liu, J. Wang, Z.-M. Liao, and D.-P. Yu, Nat. Commun. **6**, 10137 (2015).
[25] L. Schubnikow and W. J. De Haas, Nature (London) **126**, 500 (1930).
[26] P. B. Alers and R. T. Webber, Phys. Rev. **84**, 863 (1951).
[27] T. Kasuya, M. Sera, and T. Suzuki, J. Phys. Soc. Jpn. **62**, 2561 (1993).
[28] F. Y. Yang, K. Liu, K. Hong, D. H. Reich, P. C. Searson, and C. L. Chein, Science **284**, 1335 (1999).
[29] R. Xu, A. Husmann, T. F. Rosenbaum, M.-L. Saboungi, J. E. Enderby, and P. B. Littlewood, Nature (London) **390**, 57 (1997).
[30] E. Mun, H. Ko, G. J. Miller, G. D. Samolyuk, S. L. Bud'ko, and P. C. Canfield, Phys. Rev. B **85**, 035135 (2012).
[31] K. Wang, D. Graf, L. Li, L. Wang, and C. Petrovic, Sci. Rep. **4**, 7328 (2014).
[32] B. Shen, X. Y. Deng, G. Kotliar, and N. Ni, Phys. Rev. B **93**, 195119 (2016).
[33] D. S. Wu, J. Liao, W. Yi, X. Wang, P. G. Li, H. M. Weng, Y. G. Shi, Y. Q. Li, J. L. Luo, X. Dai, and Z. Fang, Appl. Phys. Lett. **108**, 042105 (2016).
[34] C. C. Xu, J. Chen, G.-X. Zhi, Y. K. Li, J. H. Dai, and C. Cao, Phys. Rev. B **93**, 195106 (2016).
[35] Y.-Y. Wang, Q.-H. Yu, P.-J. Guo, K. Liu, and T.-L. Xia, Phys. Rev. B **94**, 041103(R) (2016).
[36] Z. Wang, Y. Li, Y. Lu, Z. Shen, F. Sheng, C. Feng, Y. Zheng, and Z. Xu, arXiv:1603.01717.
[37] R. Singha, A. Pariari, B. Satpati, and P. Mandal, Proc. Natl. Acad. Sci. USA **114**, 2468 (2017).
[38] M. N. Ali, L. M. Schoop, C. Garg, J. M. Lippmann, E. Lara, B. Lotsch, and S. Parkin, arXiv:1603.09318.
[39] X. Wang, X. Pan, M. Gao, J. Yu, J. Jiang, J. Zhang, H. Zuo, M. Zhang, Z. Wei, W. Niu, Z. Xia, X. Wan, Y. Chen, F. Song, Y. Xu, B. Wang, G. Wang, and R. Zhang, Adv. Electron. Mater. **2**, 1600228 (2016).
[40] F. F. Tafti, Q. D. Gibson, S. K. Kushwaha, N. Haldolaarachchige, and R. J. Cava, Nat. Phys. **12**, 272 (2015).
[41] S. S. Sun, Q. Wang, P.-J. Guo, K. Liu, and H. C. Lei, New J. Phys. **18**, 082002 (2016).
[42] N. Kumar, C. Shekhar, S.-C. Wu, I. Leermakers, O. Young, U. Zeitler, B. Yan, and C. Felser, Phys. Rev. B **93**, 241106(R) (2016).
[43] Q. Yu, Y. Wang, R. Lou, P. Guo, S. Xu, K. Liu, S.-C. Wang, and T.-L. Xia, Europhys. Lett. **119**, 17002 (2017).
[44] O. Pavlosiuk, P. Swatek, and P. Wiśniewski, Sci. Rep. **6**, 38691 (2016).
[45] N. Wakeham, E. D. Bauer, M. Neupane, and F. Ronning, Phys. Rev. B **93**, 205152 (2016).

[46] N. Alidoust, A. Alexandradinata, S.-Y. Xu, I. Belopolski, S. K. Kushwaha, M. Zeng, M. Neupane, G. Bian, C. Liu, D. S. Sanchez, P. P. Shibayev, H. Zheng, L. Fu, A. Bansil, H. Lin, R. J. Cava, and M. Z. Hasan, arXiv:1604.08571.

[47] Q. N. Xu, Z. Song, S. Nie, H. M. Weng, Z. Fang, and X. Dai, Phys. Rev. B **92**, 205310 (2015).

[48] R. Lou, J. Z. Ma, Q. N. Xu, B. B. Fu, L. Y. Kong, Y.-G. Shi, P. Richard, H.-M. Weng, Z. Fang, S. S. Sun, Q. Wang, H.-C. Lei, T. Qian, H. Ding, and S.-C. Wang, Phys. Rev. B **93**, 241104(R) (2016).

[49] L. M. Schoop, M. N. Ali, C. Straßer, A. Topp, A. Varykhalov, D. Marchenko, V. Duppel, S. S. P. Parkin, B. V. Lotsch, and C. R. Ast, Nat. Commun. **7**, 11696 (2016).

[50] M. Zeng, C. Fang, G. Chang, Y.-A. Chen, T. Hsieh, A. Bansil, H. Lin, and L. Fu, arXiv:1504.03492.

[51] L. K. Zeng, R. Lou, D. S. Wu, Q. N. Xu, P. J. Guo, L. Y. Kong, Y. G. Zhong, J. Z. Ma, B. B. Fu, P. Richard, P. Wang, G. T. Liu, L. Lu, Y.-B. Huang, C. Fang, S. S. Sun, Q. Wang, L. Wang, Y.-G. Shi, H. M. Weng, H.-C. Lei, K. Liu, S.-C. Wang, T. Qian, J.-L. Luo, and H. Ding, Phys. Rev. Lett. **117**, 127204 (2016).

[52] R. Lou, B. B. Fu, Q. N. Xu, P. J. Guo, L. Y. Kong, L. K. Zeng, J. Z. Ma, P. Richard, C. Fang, Y.-B. Huang, S. S. Sun, Q. Wang, L. Wang, Y.-G. Shi, H. C. Lei, K. Liu, H. M. Weng, T. Qian, H. Ding, and S.-C. Wang, Phys. Rev. B **95**, 115140 (2017).

[53] P.-J. Guo, H.-C. Yang, B.-J. Zhang, K. Liu, and Z.-Y. Lu, Phys. Rev. B **93**, 235142 (2016).

[54] Y. K. Luo, R. D. McDonald, P. F. S. Rosa, B. Scott, N. Wakeham, N. J. Ghimire, E. D. Bauer, J. D. Thompson, and F. Ronning, Sci. Rep. **6**, 27294 (2016).

[55] J. Jiang, F. Tang, X. C. Pan, H. M. Liu, X. H. Niu, Y. X. Wang, D. F. Xu, H. F. Yang, B. P. Xie, F. Q. Song, P. Dudin, T. K. Kim, M. Hoesch, P. K. Das, I. Vobornik, X. G. Wan, and D. L. Feng, Phys. Rev. Lett. **115**, 166601 (2015).

[56] M. N. Ali, J. Xiong, S. Flynn, J. Tao, Q. D. Gibson, L. M. Schoop, T. Liang, N. Haldolaarachchige, M. Hirschberger, N. P. Ong, and R. J. Cava, Nature (London) **514**, 205 (2014).

[57] See Supplemental Material at http://link.aps.org/supplemental/10.1103/PhysRevB.96.241106 for ARPES and calculation methods, original Hall resistivity data at different temperatures, and fitting of the Hall conductivity at $T = 1.8$K with two-carrier model, calculated bulk band structures along more high-symmetry lines, EDCs of β_2 and a quantitative analysis on the gap between β_1 and β_2, more studies on the open character of the out-of-plane FSs, determination of the Z_2 invariant, angular-dependent MR measurements and discussions on the anisotropy of MR, etc.

[58] J. Wang, L. Li, W. You, T. Wang, C. Cao, J. Dai, and Y. Li, Sci. Rep. **7**, 15669 (2017).

[59] Compared with the experimental FS topology, the additional FSs in slab calculations possibly come from the hybridization between the wave functions of the topmost unit cell and the rest of the unit cells, because the coherence length of atomic wave functions can reach to multiple unit cells. The projected spectral weight of these states is relatively weak and thus cannot be clearly identified in the experiments. The matrix element effect may also contribute to this issue to some extent.

[60] V. N. Strocov, J. Electron Spectrosc. Relat. Phenom. **130**, 65 (2003).

[61] H. Kumigashira, H.-D. Kim, A. Ashihara, A. Chainani, T. Yokoya, T. Takahashi, A. Uesawa, and T. Suzuki, Phys. Rev. B **56**, 13654 (1997).

[62] H. Kumigashira, H.-D. Kim, T. Ito, A. Ashihara, T. Takahashi, T. Suzuki, M. Nishimura, O. Sakai, Y. Kaneta, and H. Harima, Phys. Rev. B **58**, 7675 (1998).

[63] X. H. Niu, D. F. Xu, Y. H. Bai, Q. Song, X. P. Shen, B. P. Xie, Z. Sun, Y. B. Huang, D. C. Peets, and D. L. Feng, Phys. Rev. B **94**, 165163 (2016).

[64] D. Takane, Z. Wang, S. Souma, K. Nakayama, C. X. Trang, T. Sato, T. Takahashi, and Y. Ando, Phys. Rev. B **94**, 121108(R) (2016).

[65] Although the ARPES spectra in principle reflects the electronic states integrated over a wide k_z region of bulk BZ, in reality the electronic states at $k_z = 0$ and π have main contributions [62, 64].

[66] A. Damascelli, Phys. Scr., T **109**, 61 (2004).

[67] P. Richard, T. Qian, and H. Ding, J. Phys.: Condens. Matter **27**, 293203 (2015).

[68] The SS is not topologically protected because of the trivial Z_2 index discussed below and may be merged into the bulk continuum spectra by small surface perturbations. Thus, the SS is not well reproduced in the calculated FSs in Fig. 1(e).

[69] A. A. Abrikosov, *Fundamentals of the Theory of Metals* (North-Holland, Amsterdam, 1988).

[70] J. Singleton, *Band Theory and Electronic Properties of Solids* (Oxford University Press, New York, 2001).

[71] L. Fu, C. L. Kane, and E. J. Mele, Phys. Rev. Lett. **98**, 106803 (2007).

[72] A. B. Pippard, *Magnetoresistance in Metals* (Cambridge University Press, Cambridge, 1989).

[73] N. W. Ashcroft and N. D. Mermin, *Solid Sate Physics* (Holt, Rinehart and Winston, New York, 1976).

[74] J. M. Ziman, *Principles of the Theory of Solids*, 2nd ed. (Cambridge University Press, New York, 1972).

[75] H. Takahashi, R. Okazaki, Y. Yasui, and I. Terasaki, Phys. Rev. B **84**, 205215 (2011).

[76] B. Xia, P. Ren, A. Sulaev, P. Liu, S. Q. Shen, and L. Wang, Phys. Rev. B **87**, 085442 (2013).

[77] H. Takatsu, J. J. Ishikawa, S. Yonezawa, H. Yoshino, T. Shishidou, T. Oguchi, K. Murata, and Y. Maeno, Phys. Rev. Lett. **111**, 056601 (2013).

[78] V. Eyert, R. Frésard, and A. Maignan, Chem. Mater. **20**, 2370 (2008).

[79] Y.-Y. Lv, B.-B. Zhang, X. Li, S.-H. Yao, Y. B. Chen, J. Zhou, S.-T. Zhang, M.-H. Lu, and Y.-F. Chen, Appl. Phys. Lett. **108**, 244101 (2016).